Optica Applicata, Vol. XLVI, No. 4, 2016
DOI: 10.5277/oa160408

Fast optoelectronic sensor of water concentration

JAKUB L. NOWAK[2], PAWEŁ MAGRYTA[1*], TADEUSZ STACEWICZ[1*], WOJCIECH KUMALA[2], SZYMON P. MALINOWSKI[2]

[1]Institute of Experimental Physics, Faculty of Physics, University of Warsaw, Pasteura 5, 02-093 Warsaw, Poland

[2]Institute of Geophysics, Faculty of Physics, University of Warsaw, Pasteura 7, 02-093 Warsaw, Poland

[*]Corresponding author: tadstac@fuw.edu.pl

A prototype optoelectronic hygrometer, based on absorption of laser light tuned to a specific rovibronic absorption line of H_2O at 1364.68961 nm is described. Target application is meteorology, in particular precise and fast measurements of small-scale humidity fluctuations in turbulent atmospheric flows. Tests of the prototype instrument performed in the atmospheric boundary layer have proven the advantage of this optoelectronic sensor over typical, commercially available UV hygrometers designed for similar applications.

Keywords: humidity, hygrometer, laser spectroscopy, absorption.

1. Introduction

Water vapor belongs to the main components of the atmosphere. Despite relatively low contribution to the overall mass of air, it plays a vital role in shaping weather and climate. Its optical properties affect radiative transfer making it the greenhouse gas of greatest importance. The evergoing transitions between three different phases of water result in formation of clouds, rainfalls and latent heat release.

Highly inhomogeneous distribution of water in the atmosphere poses a serious challenge for proper measurements of the vapor concentration because the mixing ratio can change by orders of magnitude on short length scales. Indeed, substantial gradients of H_2O concentration are observed in regions where air masses of different origin mix, *e.g.*, at cloud-clear air interfaces [1] or close to water vapor sources in the atmospheric boundary layer [2]. Thus, fast response stable humidity sensors are necessary to study such processes.

For stationary systems aimed at measuring vapor fluxes in the atmospheric boundary layer, the sampling rate of at least 10 Hz is required to reach spatial resolution of 1 m,

assuming 10 m/s wind speed. To achieve similar resolution in space using moving platforms, appropriately faster sampling needs to be used. For instance, a research aircraft with the speed of roughly 50–200 m/s should be equipped with the sensor capable of sampling with the rate of at least 100 Hz. However, the resolution mentioned is still not satisfactory for many applications, *e.g.*, studying cloud microphysics and thermodynamics [3] (in particular activation of cloud condensation nuclei, droplet growth, precipitation formation) where reaching Kolmogorov length scale (*i.e.*, the smallest scale in turbulent flow ~1 mm) is desirable.

The variety of instruments has been developed to measure water vapor concentration in air. Yet, the time resolution of widespread electronic capacitive or resistive hygrometers and dew point sensors lays typically in the range 10–100 s [4]. In consequence, only optical systems are able to meet the fast response demand. Several professional hygrometers based on the light absorption in UV range are available, *e.g.*, Lyman-α hygrometer [5] and KH20 Krypton hygrometer [6]. Both can sample with the rate up to 100 Hz. Nevertheless, inconveniences arising from the method, like drift of the source intensity or contamination of the windows made of hygroscopic materials, have to be overcome by incessant calibration or by baselining the high-frequency output to the humidity values provided by a slower, but stable, hygrometer.

In this paper we describe the new optoelectronic fast infrared hygrometer (FIRH), designed for independent measurements of water vapor concentration in air, based on the absorption of laser light tuned to specific rovibronic line of H_2O molecule in the near infrared range. In Section 2, we briefly explain the principle of operation. This is followed by detailed description of the instrument in Section 3 and review of calibration and signal processing techniques in Section 4. In Section 5, the results of test measurements and comparison with other sensors are demonstrated. The comparison and capabilities of our system are then discussed in Section 6 and conclusions drawn in Section 7.

2. Principles

Absorption spectrum of H_2O molecules in near- and mid-IR range (Fig. 1) consists of several bands. Each band is composed of series of narrow lines corresponding to quantum transitions between rovibronic levels of main electronic state of H_2O molecule. While selecting the most appropriate wavelength to use for H_2O detection one ought to take into account the value of absorption cross-section as well as the state of the art, *i.e.*, existence and accessibility of necessary components along with the absorption spectra of other atmospheric constituents, to exclude possible interference.

The highest values of the cross-section in the near- to mid-IR range can be found in the band around 5.93 μm. However, construction of a water vapor sensor based on these transitions, would be comparatively complicated due to the necessity of using specialized optical materials and photodetectors as well as expensive quantum cascade lasers. The next band, located in shorter wavelengths around 2.67 μm, includes the lines

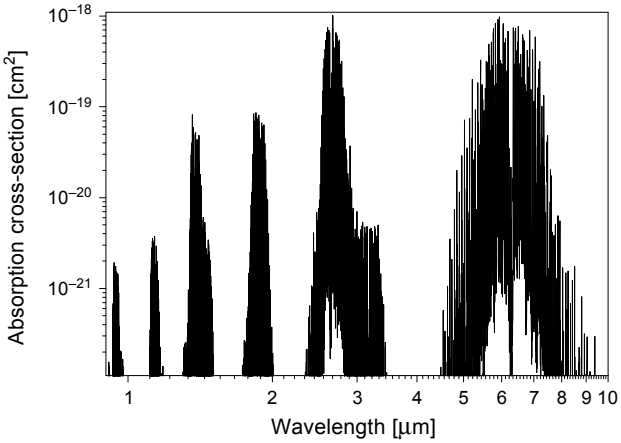

Fig. 1. Water vapor absorption spectrum in mid-IR for normal atmosphere [7].

of comparable cross-section. While common optic materials and diode lasers might be applied in this range, suitable fiber solutions (couplers, modulators, *etc*.) still need to be improved. From this point of view, the absorption band around 1.36 μm seems to be much more convenient, since diode lasers, photodetectors and fiber optics instruments are easily available and relatively inexpensive. The highest value of the cross-section in this band, 5.78×10^{-19} cm^2, is reached for the wavelength 1364.6896 nm (Fig. 2).

Shapes of spectral lines in the atmosphere are mainly determined by collisions of the absorbing molecules with air particles [8]. In rough approximation, the line profiles are described by Voigt functions; however are still a matter of investigation [9, 10]. Their parameters are collected in databases such as HITRAN or ESA [7]. The shapes depend on air pressure and temperature as well as on H_2O concentration (selfbroadening).

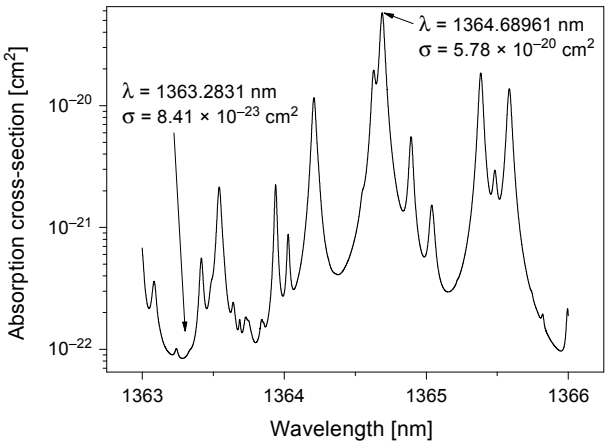

Fig. 2. Water vapor absorption spectrum around 1364 nm in normal atmosphere [7].

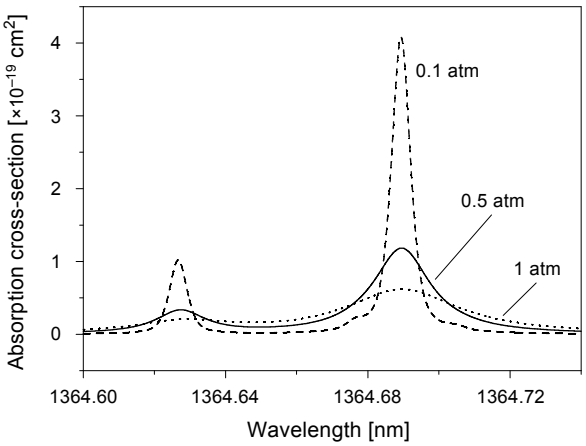

Fig. 3. Shapes of 1364.6896 nm H_2O absorption line at various air pressures.

The profiles of 1364.6896 nm line for different conditions are shown in Fig. 3. The width of the line equals approximately 0.05 nm in standard atmosphere. The line width decreases with diminishing pressure while the peak cross-section rises. For a typical range of pressure values in the atmosphere the line width decrease and the peak cross-section rise are inversely proportional to the drop of air particles concentration. The influence of atmospheric temperature on the line shape is negligible within the range 220–320 K and no pressure line-shift is observed. However the load of water vapor already present in the atmosphere, typically 10^{17} cm^{-3}, changes the line profile by several percent. All the phenomena mentioned here must be taken into account at final data elaboration.

From the careful analysis of the line shape presented in Fig. 3 one can draw a conclusion that optical measurement of water vapor concentration requires using of a single -mode laser with the wavelength precisely tuned to the line peak. For instance, in order to achieve precision of measurement better than 3% at the pressure of 380 hPa, a stability of laser wavelength better than 0.003 nm is necessary. Moreover, exact laser tuning to water line peak provides the opportunity to avoid the interference of the measurement result by other components, contained in atmosphere, primarily carbon dioxide.

3. Instrument – sensor construction

The scheme of FIRH prototype sensor is presented in Fig. 4. Single-mode semiconductor laser (Toptica, DL100) serves as a source of monochromatic light with desired wavelength. The laser beam is conducted with a fiber and split twice with the couplers. Coupler 1 directs a portion of the beam (about 1% in intensity) into the reference cell of tuning system.

The cell is filled with air saturated with water vapor and kept in stable temperature of 50°C. The H_2O concentration inside reaches 2.63×10^{18} cm^{-3} [11]. Periodic vari-

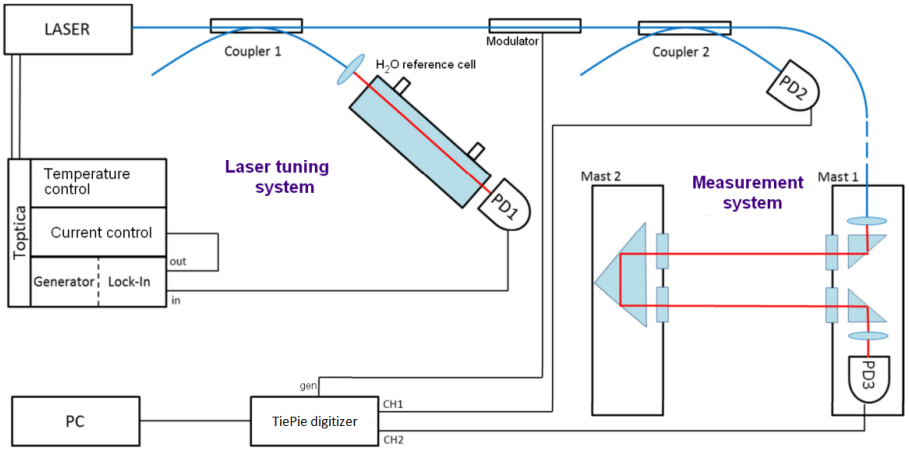

Fig. 4. Scheme of the setup. Fibers sketched in blue, light beam in red, appropriate cabling in black.

ation of laser wavelength across the absorption line is induced by sinusoidal changes in laser diode current. The variation is small in comparison with the line width. Its frequency is of about 3 kHz. That provides the amplitude modulation of the beam passing through the cell which is registered with a photodiode PD1. After demodulation with a lock-in amplifier, the correction signal, proportional to the slope of the absorption spectrum, is produced. The signal is added to the laser diode current. Such feedback loop stabilizes the laser wavelength to the peak of the line with precision of about 3×10^{-4} nm.

The main beam leaving the coupler 1 is sent to a modulator, providing the opportunity of amplitude light modulation. Coupler 2 sends a portion of it (about 10%) to another photodiode (PD2) which monitors the laser power. The dominant beam is guided from coupler 2 to measurement masts mounted outside the building. Inside the mast 1 the beam leaves the fiber through a collimator and is directed into free atmosphere. Inside the mast 2 the beam is turned back with a Dove prism so it passes twice the distance between the masts (25 cm). Finally the intensity of the beam is measured with the photodiode PD3. In order to reduce the influence of atmospheric conditions on properties and alignment of optical elements, the interiors of the masts are isolated from ambient air and the temperature inside is maintained at a constant level.

The concentration of H_2O molecules n is determined according to the Lambert –Beer law

$$n = \frac{1}{2L\sigma} \log\left(k \frac{V_{\mathrm{PD2}}}{V_{\mathrm{PD3}}}\right) \tag{1}$$

where σ denotes the absorption cross-section, L – the distance between the masts, V_{PD2} and V_{PD3} – signals from the photodiodes PD2 and PD3, respectively, while k is the calibration constant described in Section 4.

4. Calibration and signal processing

Signals generated by photodiodes PD2 and PD3 are recorded with a 12 bit digitizer (TiePie, HS5) and sent to a PC. Two strategies of signal acquisition were proposed:

i) with the modulator deactivated – to record DC signals with high sampling rate (100 kHz) and apply the averaging to reduce noise and eliminate the influence of wavelength oscillations used in laser tuning system,

ii) with the amplitude modulated beam – to use the digitizer as a two channel lock-in voltmeter and employ self-prepared software for diode signals registration.

Both methods enabled to determine V_{PD2} and V_{PD3} values. The latter approach exhibits better noise reduction. Satisfactory performance was achieved for selected modulation frequency of 2 kHz and final data averaging over 0.01 s.

As follows from Eq. (1), in order to calculate water vapor concentration using the Lambert–Beer law, one needs to define the ratio of the intensities of the initial and attenuated beam. However, these signals are affected by the parameters which are difficult to determine, *i.e.*, the photodiode sensitivity as well as the transmission properties of the couplers and other optical elements. That requires evaluation of the apparatus constant. Its value was found by measurement of the light attenuation at two different wavelengths. Namely the peak absorption line 1364.6896 nm was used as the first wavelength ($\sigma_1 = 5.78 \times 10^{-20}$ cm^2) and the minimum of absorption at 1363.2831 nm ($\sigma_2 = 8.41 \times 10^{-23}$ cm^2) as a second one (see Fig. 2). Assuming that the electric signals are proportional to true light intensities, possibly with different coefficients for the photodiodes, one can use the Lambert–Beer law to write the ratio

$$\frac{V_{\mathrm{PD2}}^{(1)}}{V_{\mathrm{PD3}}^{(1)}} \frac{V_{\mathrm{PD3}}^{(2)}}{V_{\mathrm{PD2}}^{(2)}} = \frac{I_0^{(1)}}{I_L^{(1)}} \frac{I_L^{(2)}}{I_0^{(2)}} = \exp[2nL(\sigma_1 - \sigma_2)] \tag{2}$$

where $V_{\mathrm{PD}j}^{(i)}$ is the signal of j-th photodiode for i-th wavelength. The cross-section for the second wavelength σ_2 is almost 3 orders of magnitude smaller then σ_1 and hence negligible in comparison with it. For this reason, the ratio $k = V_{\mathrm{PD3}}^{(2)}/V_{\mathrm{PD2}}^{(2)}$ can be measured only once and regarded as the calibration constant which eventually leads to Eq. (1).

5. Test measurements

In order to demonstrate capabilities of the FIRH sensor we performed a series of humidity fluctuations measurements in the atmospheric boundary later at the platform belonging to Institute of Geophysics, University of Warsaw, located on the roof of the building in the middle of urban area (Pasteura 7, Warsaw). The new instrument was installed on a 4 m high stand next to a commercial Campbell Scientific KH20 ultraviolet absorption hygrometer [12] and Young 8100 V ultrasonic anemometer [13] in configuration similar to that commonly used for estimation of turbulent fluxes in the atmospheric boundary layer (see Fig. 5).

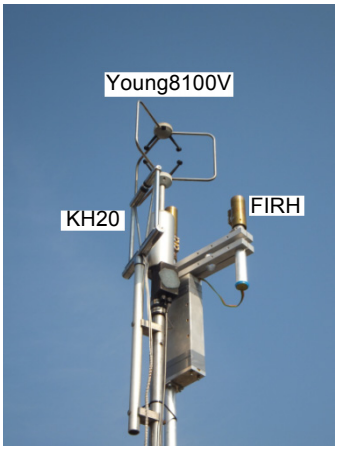

Fig. 5. Instruments arrangement on the stand used for fast response humidity measurements.

Several short- and long-term test measurements were taken in June and September 2015, including week-long session in variable meteorological conditions of early fall season. Apart from the optical hygrometers, humidity was monitored by a standard Vaisala WXT520 weather station [14], installed in the distance of about 2 m from the stand mentioned above. Some of the measurements were also accompanied by an industrial CMH-10 dew point hygrometer [15], installed in the mid-September inside a Stevenson screen, roughly in the same distance from the stand.

To enable the comparison between different instruments used, all the readings were converted into units of water vapor concentration [cm^{-3}]. For KH20 the output quantity given is absolute humidity ρ which can be converted according to the simple formula

$$n = \frac{N_\mathrm{A}}{M_\mathrm{w}}\rho \tag{3}$$

where N_A is the Avogadro constant, M_w molar mass of water molecule. Humidity sensor in Vaisala weather station and dew point hygrometer provide relative humidity R_H which can be converted with the following equation:

$$n = R_\mathrm{H}\, e_\mathrm{s}(T)\frac{N_\mathrm{A}}{RT} \tag{4}$$

where $e_\mathrm{s}(T)$ denotes the water vapor saturation pressure, $R = 8.314\ \mathrm{J\,mol^{-1}\,K^{-1}}$ is gas constant, T – temperature and N_A – Avogadro constant. Vapor pressure in saturation in Eq. (4) was estimated with the use of the approximation [16]

$$e_\mathrm{s}(T) = 611\exp\left[53.5 - \frac{6810}{T} - 5.09\log(T)\right] \tag{5}$$

In Figure 6 we present an example comparison of the instruments performance for 5 minutes long series recorded on September 15, 2015 in the morning, at 7:25 UTC

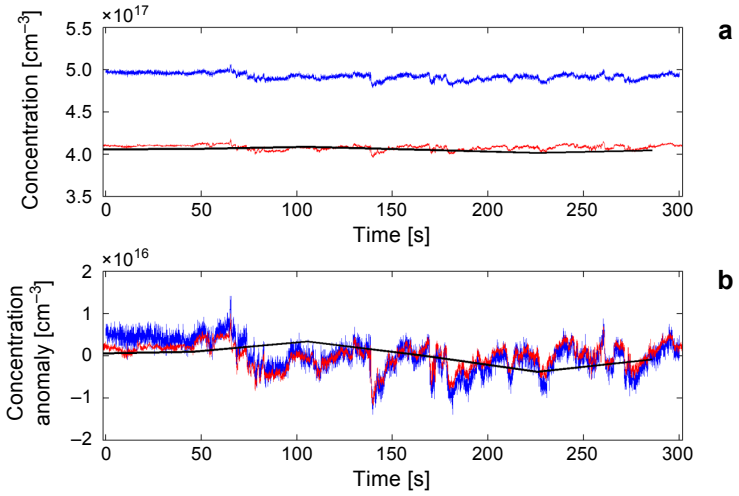

Fig. 6. Test measurement, 5 min long, recorded on Sept. 15, 2015 at 7:25–7:30 UTC (9:25–9:30 local time). Comparison of 3 instruments, FIRH (red), KH20 (blue), WXT520 (black) – absolute values (**a**) and anomaly (with the mean value subtracted) (**b**).

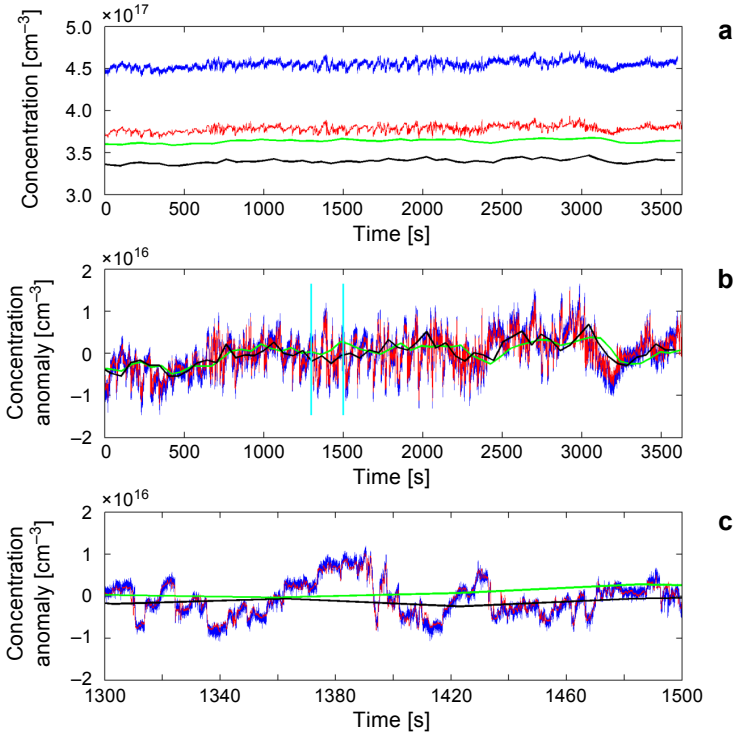

Fig. 7. Test measurement, 60 min long, recorded on Sept. 23, 2015 at 17:21–18:21 UTC (19:21–20:21 local time). Comparison of 4 instruments, FIRH (red), KH20 (blue), WXT520 (black), CMH-10 (green) – absolute values (**a**), anomaly (**b**) and anomaly for enlarged time segment marked with cyan (**c**).

(9:25 local time). In the course of this measurement the acquisition of unmodulated signals was applied (*i.e.* Sec. 4), with the sampling rate of 100 kHz and averaging over 1000 samples, which results in the final recording frequency of 100 Hz.

Another example in Fig. 7 covers 1 hour of measurements taken on September 23, 2015 in the evening, at 17:21–18:21 UTC (19:21–20:21 local time). Here, the comparison includes also data from a CMH-10 hygrometer. During this measurement we used 2 kHz amplitude modulated laser beam and lock-in integration over 20 modulation periods, which results in the final recording frequency of 100 Hz.

6. Results and discussion

In all of the collected data we observed a systematic shift between the KH20 and FIRH records. The bias was about 20%, with KH20 overestimating water vapor concentration. This can be attributed to the known property of KH20 – the effect of humidity on sensor windows. In the instruction the manufacturer writes: *The KH20 cannot be used to measure an absolute concentration of water vapor, because of scaling on the source tube windows caused by disassociation of atmospheric continuants by the ultra violet photons (...) The rate of scaling is a function of the atmospheric humidity. In a high humidity environment, scaling can occur within a few hours. That scaling attenuates the signal and can cause shifts in the calibration curve. However, the scaling over a typical flux averaging period is small. Thus, water vapor fluctuation measurements can still be made with the hygrometer*.

In some records (*cf*. Fig. 7) the bias up to 8% between the other, slow instruments and FIRH can be observed. The nature of this bias is unclear and has to be tested in future experiments. However, discrepancies between FIRH and two low frequency response sensors (WXT520 and CMH-10) are similar to these between the long response sensors themselves. Thus, in the current stage of sensor evaluation, we may state that in terms of the average water vapor concentration FIRH compares to the other sensors used in this study.

A comparison of high frequency anomalies measured with KH20 and FIRH shows a very good match of the instruments, independent of the measurement strategy (Figs. 6**b** and 7**b**, 7**c**). Both, timing and amplitude of water vapor fluctuations agree. A small drift of FIRH *vs*. KH20 can be observed in Fig. 6**b**, while no drift was observed in the course of much longer measurements shown in Fig. 7**b**. In general, some long -term (several hour) drifts of various signs were observed on long-term records. More analysis is needed to understand this feature better. One of possible explanations is the influence of solar lightening, which may affect FIRH signal.

Visual inspection of the records indicates the advantage of FIRH over KH20 in terms of the signal-to-noise ratio. Conservative estimates indicate that typically the FIRH signal-to-noise ratio is at least 2.5 times better than that of KH20. A better signal -to-noise ratio of FIRH is clearly visible in Fig. 8, which compares power spectral densities (PSDs) of water vapor fluctuations. At frequencies below 3 Hz, PSDs of records from KH20 and FIRH agree to a high level of accuracy. Both signals match –5/3 slope

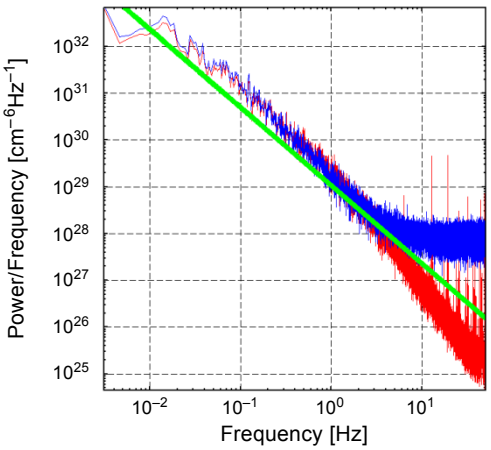

Fig. 8. Power spectral density comparison for FIRH (red) and KH20 (blue) hygrometers based on data recorded during 60 min long measurement on September 23, 2015 at 17:21–18:21 UTC (19:21–20:21 local time). Green line denotes the decay with exponent –5/3.

in log-log coordinates, as expected in measurements of passive scalar in a turbulent atmospheric boundary layer [16]. At 7 Hz the signal from KH20 reaches a noise floor. Since a documented frequency response rate of KH20 is 100 Hz, the observed white noise at frequencies above 7 Hz comes from insufficient sensitivity of the sensor to resolve small-scale humidity fluctuations in the experimental conditions.

On the contrary, FIRH at frequencies above 4 Hz shows a slight negative deflection from –5/3 slope. It is related to the construction of the sensor, exactly to 25 cm long distance between the masts, over which the signal is averaged. In the course of the measurement period, the mean wind speed was ~1 m/s. Adopting a frozen flow hypothesis, indicates that averaging over 25 cm long distance at such wind speed corresponds to 4 Hz frequency. Spatial averaging is a low-pass filtering and damps the amplitude of fluctuations of higher frequency. Nevertheless, FIRH is sensitive enough to record and measure these high-frequency fluctuations. Additional regular narrow spikes at frequencies above 6 Hz seem to have electronic nature and should be removed in the future versions of the sensor.

7. Summary

The prototype FIRH infrared hygrometer for atmospheric application was constructed and tested in the atmospheric boundary layer. The instrument survived a week long work in realistic atmospheric conditions without a noticeable effect on the performance of the sensor. Comparison to standard low-response humidity sensors used in meteorological measurements indicate a reasonable agreement between FIRH and these instruments, at least in a sense that the bias between FIRH and the other sensors is comparable to the bias between the latter themselves. Comparison to a standard, commercially available fast-response KH20 optical ultraviolet hygrometer designed for atmospheric

measurements shows a clear advantage of FIRH. The latter has a better signal-to-noise ratio and allows to measure high-frequency humidity fluctuations in the atmospheric boundary layer. Relatively long averaging length of FIRH may cause troubles in low wind speed conditions in the course of ground-based measurements. On the other hand, if the next versions of FIRH are designed for airborne operation, at 100 m/s airplane speed the records should be unaffected up to 400 Hz sampling rate. Yet, additional developments aimed at a slow drift and electric spikes removal are desirable.

Construction and test of FIRH show that optical measurement of H_2O content in atmosphere could provide absolute and sensitive results. As far as the detection limit of the absorption coefficient of about 10^{-4} cm^{-3} is available with this instrument, it provides the opportunity to register the H_2O concentration less than 2×10^{15} cm^{-3}. Fast progress in optoelectronics resulting in future application of this idea at 2.67 μm spectral range would increase this sensitivity about 20 times (Fig. 1). Further development lies in using ultrasensitive techniques of laser absorption spectroscopy [17].

Acknowledgements – This work was supported by Polish National Science Center within the research project No. N N307 635440.

References

[1] Malinowski S.P., Gerber H., Jen-La Plante I., Kopec M.K., Kumala W., Nurowska K., Chuang P.Y., Khelif D., Haman K.E., *Physics of stratocumulus top (POST): turbulent mixing across capping inversion*, Atmospheric Chemistry and Physics **13**(24), 2013, pp. 12171–12186.

[2] Högström U., *Review of some basic characteristics of the atmospheric surface layer*, Boundary-Layer Meteorology **78**(3–4), 1996, pp. 215–246.

[3] Bange J., Esposito M., Lenschow D.H., Brown P.R.A., Dreiling V., Giez A., Zöger M., *Measurement of aircraft state and thermodynamic and dynamic variables*, [In] *Airborne Measurements for Environmental Research*, M. Wendisch, J.-L. Brenguier [Eds.], Wiley-VCH Verlag, 2013, pp. 7–75.

[4] Meiklejohn W.H., *Electric hygrometer*, Transactions of the American Institute of Electrical Engineers, Part I: Communication and Electronics **77**(3), 1958, pp. 302–305.

[5] Zöger M., Afchine A., Eicke N., Gerhards M.-T., Klein E., McKenna D.S., Mörschel U., Schmidt U., Tan V., Tuitjer F., Woyke T., Schiller C., *Fast in situ stratospheric hygrometers: a new family of balloon-borne and airborne Lyman α photofragment fluorescence hygrometers*, Journal of Geophysical Research: Atmospheres **104**(D1), 1999, pp. 1807–1816.

[6] Foken T., Falke H., *Technical Note: Calibration instrument for the krypton hygrometer KH20*, Atmospheric Measurement Techniques Discussions **5**(1), 2012, pp. 1695–1715.

[7] Rothman L.S., Gordon I.E., Babikov Y., Barbe A., Chris Benner D., Bernath P.F., Birk M., Bizzocchi L., Boudon V., Brown L.R., Campargue A., Chance K., Cohen E.A., Coudert L.H., Devi V.M., Drouin B.J., Fayt A., Flaud J.-M., Gamache R.R., Harrison J.J., Hartmann J.-M., Hill C., Hodges J.T., Jacquemart D., Jolly A., Lamouroux J., Le Roy R.J., Li G., Long D.A., Lyulin O.M., Mackie C.J., Massie S.T., Mikhailenko S., Müller H.S.P., Naumenko O.V., Nikitin A.V., Orphal J., Perevalov V., Perrin A., Polovtseva E.R., Richard C., Smith M.A.H., Starikova E., Sung K., Tashkun S., Tennyson J., Toon G.C., Tyuterev Vl.G., Wagner G., *The HITRAN2012 molecular spectroscopic database*, Journal of Quantitative Spectroscopy and Radiative Transfer **130**, 2013, pp. 4–50.

[8] Demtröder W., *Laser Spectroscopy*, 3rd Ed., Springer-Verlag, Berlin, Heidelberg, New York, 2003.

[9] Lisak D., Hodges J.T., *High-resolution cavity ring-down spectroscopy measurements of blended H_2O transitions*, Applied Physics B **88**(2), 2007, pp. 317–325.

[10] LISAK D., HAVEY D.K., HODGES J.T., *Spectroscopic line parameters of water vapor for rotation-vibration transitions near 7180 cm^{-1}*, Physical Review A **79**(5), 2009, article 052507.
[11] ALDUCHOV O.A., ESKRIDGE R.E., *Improved Magnus form approximation of saturation vapor pressure*, Journal of Applied Meteorology **35**(4), 1996, pp. 601–609.
[12] https://www.campbellsci.com/kh20
[13] http://www.youngusa.com/products/6/45.html
[14] http://www.vaisala.com/en/products/multiweathersensors/Pages/WXT520.aspx
[15] http://www.czaki.pl/czaki2/plik/cmh-10-humidity-meters-in-gases-data-sheet_nn3184.pdf
[16] WARHAFT Z., *Passive scalars in turbulent flows*, Annual Review of Fluid Mechanics **32**(1), 2000, pp. 203–240.
[17] WOJTAS J., TITTEL F.K., STACEWICZ T., BIELECKI Z., LEWICKI R., MIKOLAJCZYK J., NOWAKOWSKI M., SZABRA D., STEFANSKI P., TARKA J., *Cavity-enhanced absorption spectroscopy and photoacoustic spectroscopy for human breath analysis*, International Journal of Thermophysics **35**(12), 2014, pp. 2215–2225.

Received April 16, 2016